Solar Phys (2015) 290:2507–2518
DOI 10.1007/s11207-015-0758-0

Comparison of Solar Wind Speeds Using Wavelet Transform and Fourier Analysis in IPS Data

E. Aguilar-Rodriguez[1] · J.C. Mejia-Ambriz[2,3] · B.V. Jackson[2] · A. Buffington[2] · E. Romero-Hernandez[1] · J.A. Gonzalez-Esparza[1] · M. Rodriguez-Martinez[4] · P. Hick[2] · M. Tokumaru[5] · P.K. Manoharan[6]

Received: 2 March 2015 / Accepted: 4 August 2015 / Published online: 7 October 2015

Abstract The power spectra of intensity fluctuations in interplanetary scintillation (IPS) observations can be used to estimate solar-wind speeds in the inner heliosphere. We obtain and then compare IPS spectra from both wavelet and Fourier analyses for 12 time series of the radio source 3C48; these observations were carried out at Japan's Solar-Terrestrial Environment Laboratory (STEL) facility, at 327 MHz. We show that wavelet and Fourier analyses yield very similar power spectra. Thus, when fitting a model to spectra to determine solar-wind speeds, both yield comparable results. Although spectra from wavelet and Fourier closely match each other for solar-wind speed purposes, those from the wavelet analysis are slightly cleaner, which is reflected in an apparent level of intensity fluctuations that is enhanced, being $\approx 13~\%$ higher. This is potentially useful for records that show a low signal-to-noise ratio.

Keywords Radio scintillation · Solar wind, disturbances · Waves, propagation

Radio Heliophysics: Science and Forecasting
Guest Editors: Mario M. Bisi, Bernard V. Jackson, and J. Americo Gonzalez-Esparza

✉ E. Aguilar-Rodriguez
ernesto@geofisica.unam.mx

1 Instituto de Geofisica, Universidad Nacional Autonoma de Mexico, Morelia, Mexico

2 Center for Astrophysics and Space Sciences, University of California, San Diego, 9500 Gilman Drive, La Jolla, CA 92093-0424, USA

3 SCiESMEX, Instituto de Geofisica, Universidad Nacional Autonoma de Mexico, Morelia, Mexico

4 ENES-Morelia, Universidad Nacional Autonoma de Mexico, Morelia, Mexico

5 Solar-Terrestrial Environment Laboratory, Nagoya University, Nagoya 464-8601, Japan

6 Radio Astronomy Centre, National Centre for Radio Astrophysics, Tata Institute of Fundamental Research, P.O. Box 8, Udhagamandalam (Ooty) 643001, India

1. Introduction

Radio waves become modulated in phase and amplitude after passing through solar-wind density irregularities of small-scale size ($\approx 10-500$ km). These irregularities cause a moving radiation pattern at Earth, which is observed by radio telescopes as intensity fluctuations [ΔI] of the sources at temporal scales $\approx$ one second: these fluctuations are known as interplanetary scintillation (IPS). The temporal power spectra of this IPS contain statistical information about various properties of the solar wind integrated along the line of sight (LOS): these include velocity (Scott, Coles, and Bourgois, 1983; Manoharan and Ananthakrishnan, 1990; Manoharan, 1993; Moran *et al.*, 2000), density fluctuations (Asai *et al.*, 1998; Tokumaru, Kojima, and Fujiki, 2012), turbulence spectrum (Coles and Harmon, 1978; Gapper and Hewish, 1981; Manoharan, Kojima, and Misawa, 1994), and axial ratio of the irregularities (Chashei *et al.*, 2000; Tokumaru *et al.*, 2011). Furthermore, they can reveal the apparent structure of the observed radio sources (Manoharan and Ananthakrishnan, 1990; Glubokova, Chasei, and Tyul'bashev, 2012). When the phase fluctuations [$\Delta\phi$] from IPS satisfy $\Delta\phi \ll$ one radian, the so-called weak-scattering condition, some of these properties can be extracted by modeling the power spectra. The model is constructed by a superposition of thin plasma layers perpendicular to the LOS, each layer contributing a change of $\Delta\phi$ to the wave. The point along the LOS closest to the Sun (the P-point) has the highest statistical weight, and thus the measured properties are often associated with this point. In the case of velocity, the IPS analysis estimates the outflow component observed at Earth, which results from the integration of perpendicular velocity components to the LOS that we call solar-wind speed. Information on density fluctuations is provided by a disturbance factor [g] (Gapper *et al.*, 1982), which can be calculated by integrating the observed spectrum (*e.g.* Fallows, Williams, and Breen, 2002; Manoharan *et al.*, 2000; Tokumaru, Kojima, and Fujiki, 2012).

To obtain an accurate estimate of the physical parameters in the solar wind via the IPS power spectra, two things are required: an appropriate treatment of the time series and a high signal-to-noise ratio (S/N) of the intensity fluctuations. Appropriate treatment here consists of detrending, filtering, and smoothing the data such that the resulting power spectra emphasize the characteristics from IPS and minimize the influence of external noise. A high S/N of the power spectra is necessary to identify all of the parameters via this modeling. For example, Manoharan and Ananthakrishnan (1990) argued that power spectra with S/N $>$ 25 dB above the background noise level is enough to explore all of the parameters. On the other hand, Balasubramanian *et al.* (2003) pointed out that a reliable determination of speed only requires a S/N $>$ 10 dB, while an even lower S/N can determine a reliable g. This results in more sources suitable to study g than velocities. Mejia-Ambriz *et al.* (2015) showed that the axial ratio and spectral turbulence parameters can sometimes be fixed to obtain reliable values of the solar-wind speeds, fitting the model to observed spectra with a S/N $>$ 20 dB.

1.1. Wavelet Transform Function

The wavelet transform (WT) function can be used as an alternative tool to obtain the IPS power spectra: in this case no Fourier transform is needed, and only an appropriate treatment and selection of the data is required. The WT is used in ionospheric scintillation as a detrending tool (*e.g.* Sajan *et al.*, 2012); in IPS Aguilar-Rodriguez *et al.* (2014) applied the WT to obtain the level of scintillation through the average of the intensity fluctuations [$\langle\Delta I\rangle$].

Dedicated IPS ground-based radio telescopes such as the Solar Wind Imaging Facility Telescope (SWIFT: Tokumaru *et al.*, 2011) of the Solar-Terrestrial Environment Laboratory (STEL), the Mexican Array Radio Telescope (MEXART: Gonzalez-Esparza *et al.*, 2004; Mejia-Ambriz *et al.*, 2010), the Ooty Radio Telescope (ORT: Manoharan, 2012), the Big Scanning Array (BSA) of the Lebedev Physical Institute (Chashei *et al.*, 2013), as well as antenna systems that operate on a campaign basis such as the Low-Frequency Array (LOFAR: van Haarlem *et al.*, 2013), and the European Incoherent Scatter (EISCAT: Wannberg *et al.*, 1997), among others, continually record the intensity of radio sources and their fluctuations about the mean. The quality of the IPS data depends on the S/N in the measurements and the absence of interference. In many cases, the results obtained by the IPS observations have a substantial uncertainty due to these problems. Since the IPS fluctuations are nonstationary in nature, the wavelet transform (WT) function can be used as an alternative tool to derive localized variations of IPS power. The WT provides a way to decompose a time series into time–frequency space in order to determine the dominant modes of variability and how the amplitudes of these modes vary in time. Moreover, the WT has an advantage over Fourier transforms since it can extract frequency information from a signal using variable-sized windows from the time series. As shown by Farge (1992), Torrence and Compo (1998), and De Moortel, Munday, and Hood (2014), the continuous WT of a function $[f(t)]$ is defined by the convolution of $f(t)$ with an analyzing function $[\psi(\eta)]$. The transformation is based on a scheme where the analyzing wavelet is scaled and shifted along the analyzed signal according to the following equation:

$$W(\tau, s) = \frac{1}{\sqrt{s}} \int_{-\infty}^{\infty} f(t)\psi\left(\frac{t-\tau}{s}\right)\mathrm{d}t, \tag{1}$$

where $\psi(t)$ is the analyzing wavelet, s and τ are the scale and time, respectively, and together they represent the domain of the WT. The s-variable is equal to the scale of the analyzing wavelet at every step of the transform calculation, and its reciprocal is equal to the frequency. The analyzed wavelet must satisfy some criteria. It should have finite energy and a mean value equal to zero. The nature of the signal and the information that is desired to be extracted from it define the analysis (or mother) wavelet. Several mother wavelets, such as Morlet, Paul, and the Derivative of Gaussian (DOG, also known as the Mexican hat), are commonly used in WT analysis. Basic differences appear depending on which mother wavelet is applied to a signal. De Moortel, Munday, and Hood (2014) applied the Morlet, Paul, and DOG wavelet on a simple analytical function. Their results showed that the Morlet wavelet resolves the different frequency components well, but has some overlap between their respective temporal localizations. The Paul wavelet gives a relatively sharp transition between the time localizations of the different frequency components, but the actual frequency resolution appears to be lower. The DOG wavelet has relatively few oscillations in a much wider temporal domain. For IPS purposes, the Morlet wavelet is the appropriate option because it ensures a good frequency resolution compared with the other two mother wavelets. The Morlet wavelet consists of a plane wave modulated by a Gaussian: $\psi(\eta) = \pi^{-1/4} e^{\mathrm{i}\omega_0\eta} e^{-\eta^2/2}$, where ω_0 is the nondimensional frequency, taken here to be six, to fullfil the condition of the mean value of the function equal to zero. The smallest scale of the wavelet is set to $2\mathrm{d}t$ in order to obtain the same Nyquist frequency as in the raw time series.

To exemplify what IPS observations of compact extragalactic radio sources look like after applying the WT, we considered records of the 3C48 radio source observed by STEL and ORT on 24 May 2013, and by MEXART on 23 May 2013. Both ORT and STEL radio telescopes operate at a frequency of 327 MHz with the same signal sampling rate (20 ms) as

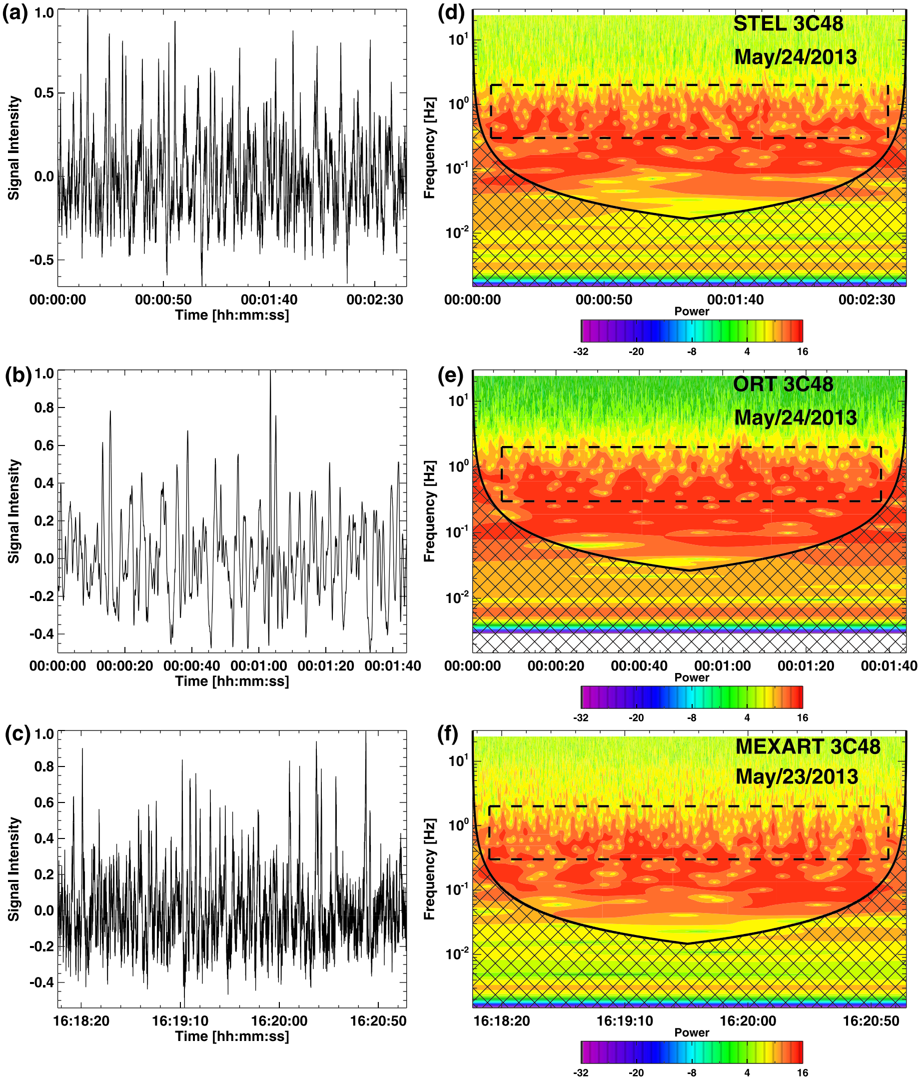

Figure 1 Transit of the radio source 3C48 observed by the (a) STEL, (b) ORT, and (c) MEXART radio telescopes. (d), (e), and (f) show the WT applied to these time series, which allows us to identify intensity fluctuations due to IPS in the on-source region. The dashed-line boxes indicate the frequency range where IPS is commonly observed (*i.e.* from 0.3 Hz up to 2 Hz). The cross-hatched regions represent the cone of influence (COI).

MEXART, which operates at a frequency of 140 MHz. These radio telescopes are located at different longitudes, so the best way to compare these observations is to choose the record registered by MEXART one day before those obtained by STEL and ORT. We removed any potential low-frequency trend in the time series by subtracting the running mean of $\approx$ ten seconds, which sums ≈ 500 data points at a 0.02-second resolution. This procedure, which acts as a high-pass filter, reduces the data contamination due to ionospheric scintillations when they are present. Figures 1a – c show the transit of the radio source 3C48 observed by these three radio telescopes, where the described procedure was applied. Figures 1d – f show the WT applied to these subtracted IPS time series. We used the Torrence and Compo (1998) code to construct the wavelet. The mother wavelet applied was the Morlet because, as we mentioned previously, it gives a better frequency resolution. Since the Torrence and Compo (1998) code takes a Fourier transform of the data to compute the WT at a given scale [s] for all n temporal variations simultaneously, it speeds up the computations. However, as the Fourier transform is cyclic, and the IPS time series are of finite length, this introduces errors at the edges of the transform. The cone of influence (COI) is the region of the wavelet spectrum within which edge effects become important. This COI is defined so that the wavelet power for a discontinuity at the edges decreases by a factor e^{-2}. Regions of the WT that are inside the area formed by the time axis and the cone of influence are subject to these edge effects and are considered unreliable. In Figures 1d – f the dashed-line box contains the window of the IPS spectral frequency, which is typically from 0.3 to 2 Hz. The intensity fluctuations due to IPS are clearly seen inside this box, and undoubtedly outside of the cross-hatched regions that represent the COI.

We here use the WT to derive IPS power spectra and evaluate the capability of the WT spectra to provide solar-wind speeds. We also employ spectra previously obtained from a Fourier analysis method (Mejia-Ambriz *et al.*, 2015) for a direct comparison. Additionally, in our case the WT method provides cleaner spectra, with a higher S/N than those obtained from the Fourier analysis.

2. Observations

The IPS time series for this study are twelve observations of the source 3C48 with the parabolic SWIFT array from STEL at 327 MHz (for general characteristics of SWIFT see Tokumaru *et al.*, 2011); these are recorded with a sampling rate of 50 Hz for about 5.25 minutes. Observations were taken in the weak-scattering region during both the minimum and maximum of Solar Cycle 24, with the P-point located at heliocentric distances ranging from 0.37 to 0.45 AU. These time series were analyzed by Mejia-Ambriz *et al.* (2015), where solar-wind speeds that result from fitting a model to the observed power spectra using Fourier analysis were shown to agree with speeds measured more directly via multi-station IPS measurements using a cross-correlation between the separate stations. These power spectra also match the shape expected from the model.

3. Characteristics of IPS Power Spectra

IPS power spectra are often presented in a log–log plot as shown in Figure 2. Typically, under average solar-wind conditions at meter-wavelength observations, these consist of a nearly constant high power at low frequencies, with a reduction beginning at about 1 Hz (the Fresnel knee) and continuing until the power has dropped to the white-noise level at high frequencies. From the theory of scintillation in weak scattering, two functions play an important role in the shape of the spectra: the Fresnel filter and the power spectrum of density fluctuations [$\Phi_{\Delta N}(k_x, k_y, k_z)$]. Thus, in an x–y-plane perpendicular to the LOS at distance z, a layer of thickness Δz at observing wavelength λ produces the spectrum

$$\Delta P(k_x, k_y) \propto \sin^2\left(\frac{k^2 \lambda z}{4\pi}\right) \Phi_{\Delta N}(k_x, k_y, k_z = 0) \Delta z, \tag{2}$$

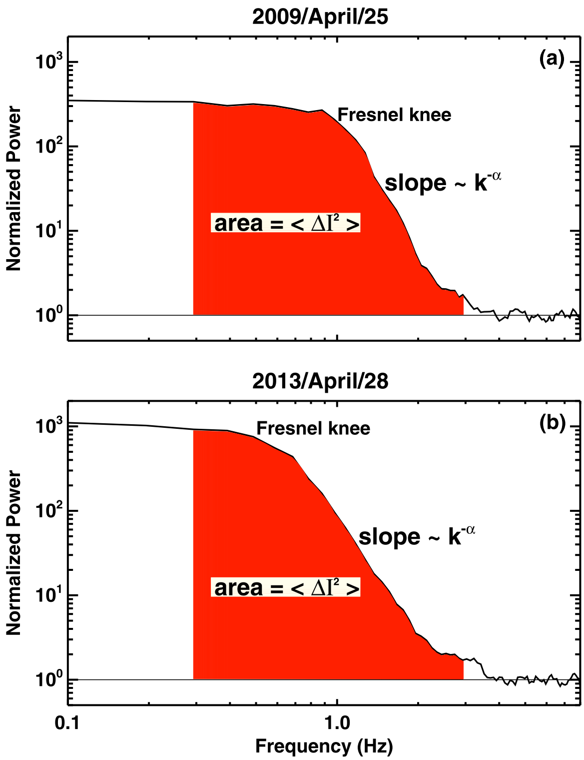

Figure 2 Two power spectra of 3C48 at 327 MHz normalized to unity at the high-frequency part of the spectrum (white-noise level) taken at the indicated dates. The IPS contribution (shaded red) contains values for solar-wind speed (Fresnel knee location), turbulence spectrum of density (slope, $-\alpha$), and IPS g.

where k_x, k_y, k_z are the components of the spatial wavenumber with $k = (k_x^2 + k_y^2)^{1/2}$. k_x is related to solar-wind speed $[V]$ and time-series analysis frequency $[f]$ by $k_x = 2\pi f/V$. To illustrate the general effect of $\Phi_{\Delta N}$, we assume here the simple case

$$\Phi_{\Delta N} \propto R^{-4} k^{-\alpha}, \tag{3}$$

where R is the heliocentric distance to the intersection between the LOS and the particular layer. Figure 2 shows two examples of observed power spectra including contributions from all layers along the LOS. The first maximum and second minimum of the Fresnel function produces the Fresnel knee; the turbulence spectrum governs the slope of the knee. However, near the onset of the white noise (below about two, in the normalized power, see Figure 2) the slope due to the turbulence is blurred when it is combined with the white noise. The solar-wind speed derived from the power spectrum is mainly determined by the location of the knee.

Another important parameter that can be obtained from the spectra is the disturbance factor $[g]$ for each heliocentric distance $[r]$ to the P-point,

$$g^2 = \frac{\langle \Delta I^2(r) \rangle}{\overline{\langle \Delta I^2(r) \rangle}}, \tag{4}$$

where $\overline{\langle \Delta I^2(r) \rangle}$ is the expected level of scintillation for a particular source at that distance. Thus, g is the ratio of a particular level of scintillation in a given sample, to its long-term average $[\overline{\langle \Delta I^2(r) \rangle}]$.$\langle \Delta I^2 \rangle$ is obtained from the spectrum by

$$\langle \Delta I^2 \rangle = \int P(f)\,\mathrm{d}f. \tag{5}$$

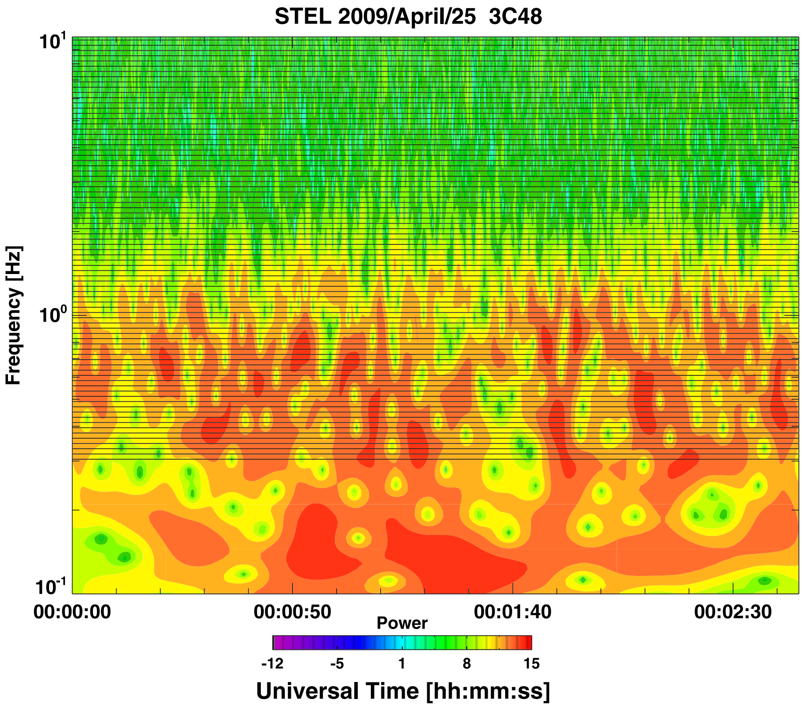

Figure 3 Example of the wavelet decomposition (time–frequency) applied to a detrended and relatively clean time series of about 165 seconds. The frequency is shown in log scale. Each horizontal line corresponds to one point of the averaged power spectrum. Figure 2a shows the power spectrum from a Fourier analysis of this.

This integration is taken along the interval of frequency f; here we used 0.3 to 3 Hz (the red shaded portions of Figure 2. The interval chosen to include the Fresnel knee for all 12 analyzed time series).

4. Data Analysis

To obtain the power spectra of each analysis, WT and Fourier, we followed a general procedure. The time series were first detrended to remove low-frequency fluctuations, which can arise due to ionospheric scintillation or other non-IPS factors as explained in the introduction section. Then sections of the time series identified with spikes (commonly some sort of external interference) were removed, and finally we obtained the power spectra from the remaining detrended data.

For the case of WT, the trend and low-frequency fluctuations in the time series were removed by subtracting a running mean over ten seconds, and then the WT was applied. Figure 3 shows the WT applied to a transit of 3C48 observed on 25 April 2009 (power spectra of this observation are shown in Figures 2a and 4). The power of the signal is represented as a function of time and frequency. This decomposition of the time series into time–frequency space gives an array of 255 frequency channels, covering a range from ≈ 0.001 Hz up to ≈ 24.2 Hz. By considering the frequency range from 0.3 Hz up to 10 Hz (as shown in Figure 3), we obtained an array of 81 frequency channels. The horizontal lines in Figure 3

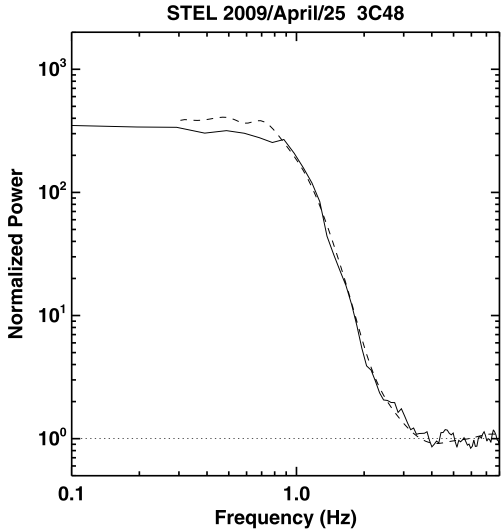

Figure 4 Power spectra normalized to unity at the white-noise level. The dashed line represents the spectrum obtained with the WT (Figure 3). The solid line shows the spectrum with the Fourier transform (Figure 2a).

represent these 81 frequency channels. Spikes in the data were identified in the wavelet representation as high-power vertical strips; the spikes can be skipped by choosing windows whose horizontal sizes contain the high-power regions, and then these regions were eliminated from further analysis (see Aguilar-Rodriguez *et al.*, 2014). To construct the power spectrum, an average power was computed at each frequency channel. We modified the Torrence and Compo (1998) code to perform this procedure by adding a subroutine that graphically eliminates spikes on the wavelet and then computes the average power at each frequency channel with the data free of spikes, if present, and also outside of the COI. Figure 4 shows the power spectrum obtained from Figure 3, together with the corresponding one from the Fourier analysis.

For the Fourier analysis (see details in Mejia-Ambriz *et al.*, 2015), we divided the time series into subintervals of 10.24 seconds (512 data points) and then took the power spectrum of each subinterval via a fast Fourier transform (FFT). Spectra containing interference (spikes), with high noise at high frequencies, were discarded. Finally, the remaining spectra were averaged together. Taking subintervals this way functions as detrending, and it avoids high power values at low frequencies ≈ 0.1 Hz. Integration from 2.5 Hz to 10 Hz estimates the noise level induced by interference for each individual power spectrum; spectra whose noise level is twice as high or more than the less noisy spectra were discarded.

To obtain the solar-wind speeds, we applied the model fitting to the spectra in the region from ≈ 0.3 to ≈ 2 Hz, as previously (Mejia-Ambriz *et al.*, 2015) including error estimates, for the spectra from FFT. Then we applied the same methodology to the WT power spectra. Additionally, we measured the area below the power spectra from 0.3 to 3 Hz to calculate Equation (5); for the fitting we used a frequency range narrower than that used to calculate the area.

5. Summary and Results

We here presented a wavelet-analysis alternative for obtaining IPS power spectra and, via fitting of a model, its use in calculating solar-wind speeds. We applied this technique to

Table 1 Solar-wind speeds and area below the power spectra calculated from wavelet and Fourier analysis for 3C48 observations at 327 MHz with STEL. Speeds calculated by cross-correlation (multi-station) are included.

Date	WT speed [$\mathrm{km\,s^{-1}}$]	FFT speed [$\mathrm{km\,s^{-1}}$]	Multi-station speed [$\mathrm{km\,s^{-1}}$]	WT $\langle \Delta I^2 \rangle$	Fourier $\langle \Delta I^2 \rangle$
21 April 2009	625 ± 100	630 ± 95	672 ± 4	245	198
23 April 2009	660 ± 57	655 ± 62	643 ± 2[a]	235	223
24 April 2009	640 ± 75	655 ± 45	627 ± 5	286	254
25 April 2009	655 ± 52	670 ± 32	625 ± 0[a]	288	253
28 April 2009	615 ± 122	625 ± 115	610 ± 4	186	156
8 May 2012	380 ± 85	380 ± 55	382 ± 10	302	247
9 May 2012	420 ± 102	430 ± 57	424 ± 22	182	209
29 March 2013	395 ± 67	395 ± 57	380 ± 0[a]	74	62
8 April 2013	335 ± 60	340 ± 60	394 ± 4	150	134
26 April 2013	450 ± 95	450 ± 65	749 ± 23	145	132
27 April 2013	430 ± 77	415 ± 77	421 ± 2[a]	291	250
28 April 2013	380 ± 65	390 ± 50	375 ± 23	440	374

[a]The minimum uncertainty here is four, even though the discrepancy between the multi-station values may sometimes be smaller.

twelve time series of 3C48 IPS observations at 327 MHz. Furthermore, we calculated $\langle \Delta I^2 \rangle$ using Equation (5) with both wavelet and Fourier analyses. Table 1 and Figure 5 show the values of solar-wind speeds: solar-wind speeds and estimated errors from WT and FFT methods match with negligible differences (see panel c in Figure 5), reaching an almost perfect one-to-one correlation, and exhibiting a similar error margin. The very similar speeds from both WT and FFT results provide two similar comparisons: WT (single-station) *vs.* cross-correlation (multi-station) as seen in Figure 5a, and Fourier (single-station) *vs.* cross-correlation (multi-station) in Figure 5b. This shows that WT provides reliable solar-wind speeds for the present data. Only one data point does not match between single and multi-station methods, corresponding to the point far away from the dashed line in Figures 5a and 5b, which was obtained on 26 April 2013 and is listed in Table 1: this discrepancy might be due to the influence of a nearby coronal mass ejection that might change the assumed parameters in the model used here (Mejia-Ambriz *et al.*, 2015). The two last columns of Table 1 and Figure 6 show the level of scintillation using WT and Fourier. Power spectra from the wavelet analysis tend to have a better S/N, which in turn is reflected in the higher $\langle \Delta I^2 \rangle$ values, which exceed those from the Fourier analysis by an average of 13 %. This difference seems systematic with a correlation of 0.97, and as a consequence, the g-values that would result from each method appear to scale with one another for each data set. The use of WT to calculate the IPS power spectra has two advantages over the Fourier method: WT spectra can have a higher resolution, and contaminated data in the time series are easily removed by selecting windows in the time–frequency representation (see Aguilar-Rodriguez *et al.*, 2014). This results in less data loss due to contamination compared with the Fourier analysis, where a complete subinterval that is contaminated by a minor region has to be discarded. Finally, the S/N of the data used here for both Fourier and WT methods are sufficiently alike that no substantial difference exists between the speeds determined from each; in the case of lower S/N, WT may deliver a more reliable speed.

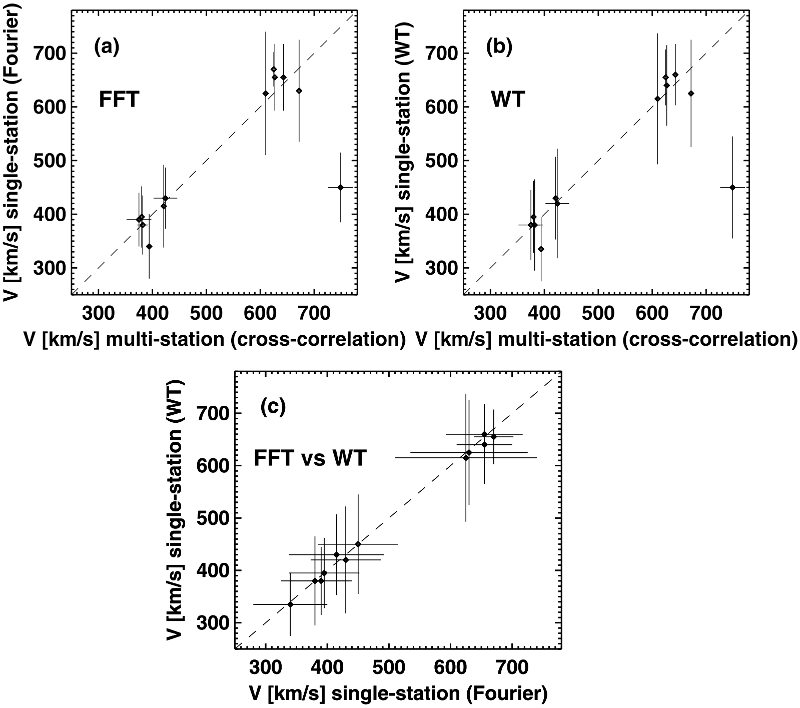

Figure 5 Comparison of solar-wind speed measurements by different methods. Panel a is taken from Mejia-Ambriz *et al.* (2015). Panels a and b are solar-wind speeds obtained by multi-station (cross-correlation) *vs.* those by single-station (model fitting to spectra from Fourier and wavelet). Panel c shows fitting speeds from wavelet *vs.* fitting from Fourier spectra.

Figure 6 Comparison of the scintillation level between spectra obtained from Fourier and wavelet methods [arbitrary units]. Spectra from the wavelet method tend to have more robust power, which is reflected in slightly higher levels of scintillation than those from the Fourier method.

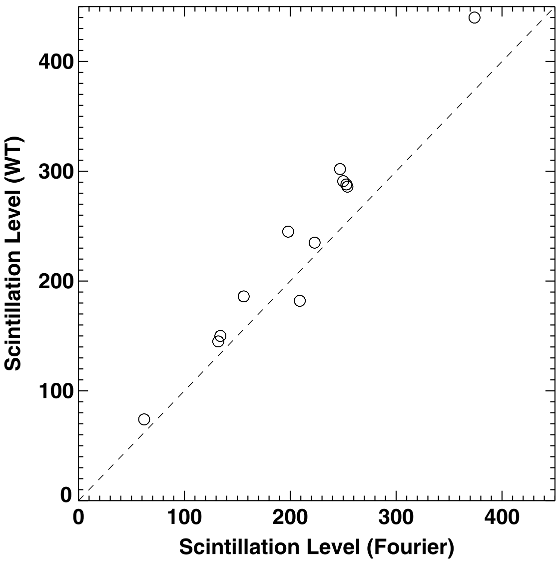

Acknowledgements The STEL IPS observations were carried out under the solar-wind program of the Solar-Terrestrial Environment Laboratory (STEL) of Nagoya University. Wavelet software was provided by C. Torrence and G. Compo, and is available at URL: http://atoc.colorado.edu/research/wavelets/. E. Aguilar-Rodriguez acknowledges the DGAPA/PAPIIT project (grant: IN103615) and the CONACyT project (grant: 220981), Ernesto Andrade-Mascote, and Pablo Villanueva-Hernandez. J.C. Mejia-Ambriz acknowledges the Cátedras CONACyT project 1045: Servicio de Clima Espacial México (SCiES-MEX). B.V. Jackson and a portion of Mejia-Ambriz's stay at UCSD have been funded by NSF contract AGS-1053766 to the University of California, San Diego. B.V. Jackson has also been supported by AFOSR contract FA9550-11-1-0324. J.A. Gonzalez-Esparza thanks for the DGAPA-PAPIIT grant IN109413 and CONACyT grant 152471. M. Rodriguez-Martinez acknowledges the DGAPA-PAPIIT project IA102514 and the CONACyT Infrastructure Grant: 253691. M. Tokumaru thanks the Japan Society for the Promotion of Science (JSPS) for financial support by a Grant-in-Aid for Scientific Research (A) No. 25247079. P.K. Manoharan acknowledges partial support by the CAWSES-India Program, sponsored by ISRO.

Conflict of interest The authors declare that they have no conflicts of interest.

References

Aguilar-Rodriguez, E., Rodriguez-Martinez, M., Romero-Hernandez, E., Mejia-Ambriz, J.C., Gonzalez-Esparza, J.A., Tokumaru, M.: 2014, The wavelet transform function to analyze interplanetary scintillation observations. *Geophys. Res. Lett.* **41**, 3331. DOI.

Asai, K., Kojima, M., Tokumaru, M., Yokobe, A., Jackson, B.V., Hick, P.L., Manoharan, P.K.: 1998, Heliospheric tomography using interplanetary scintillation observations: 3. Correlation between speed and electron density fluctuations in the solar wind. *J. Geophys. Res.* **103**, 1991. DOI.

Balasubramanian, V., Janardhan, P., Srinivasan, S., Ananthakrishnan, S.: 2003, Interplanetary scintillation observations of the solar wind disappearance event of May 1999. *J. Geophys. Res.* **108**, 1121. DOI.

Chashei, I.V., Efimov, A.I., Rudash, V.K., Bird, M.K.: 2000, Anisotropy and velocity of small-scale irregularities in the region of solar-wind acceleration. *Astron. Rep.* **44**, 634. DOI.

Chashei, I.V., Shishov, V.I., Tyul'bashev, S.A., Subaev, I.A., Oreshko, V.V.: 2013, Results of IPS observations in the period near solar activity minimum. *Solar Phys.* **285**, 141. DOI.

Coles, W.A., Harmon, J.K.: 1978, Interplanetary scintillation measurements of electron density power spectrum in the solar wind. *J. Geophys. Res.* **83**, 1413. DOI.

De Moortel, I., Munday, S.A., Hood, A.W.: 2014, Wavelet analysis: the effect of varying basic wavelet parameters. *Solar Phys.* **222**, 203. DOI.

Fallows, R.A., Williams, P.J.S., Breen, A.R.: 2002, EISCAT measurements of solar wind velocity and the associated level of interplanetary scintillation. *Ann. Geophys.* **20**, 1279. DOI.

Farge, M.: 1992, Wavelet transforms and their applications to turbulence. *Annu. Rev. Fluid Mech.* **24**, 395. DOI.

Gapper, G.R., Hewish, A.: 1981, Density gradients in the solar plasma observed by interplanetary scintillation. *Mon. Not. Roy. Astron. Soc.* **197**, 209. DOI.

Gapper, G.R., Hewish, A., Purvis, A., Duffet-Smith, P.J.: 1982, Observing interplanetary disturbances from the ground. *Nature* **296**, 633. DOI.

Glubokova, S.K., Chasei, I.V., Tyul'bashev, S.A.: 2012, Small-scale solar wind density turbulence spectrum from interplanetary scintillation observations. *Adv. Astron. Space Phys.* **2**, 164. DOI.

Gonzalez-Esparza, J.A., Carrillo, A., Andrade, E., Perez-Enriquez, R., Kurtz, S.: 2004, The MEXART interplanetary scintillation array in Mexico. *Geophys. Int.* **43**, 61.

Manoharan, A.P.: 2012, Three-dimensional evolution of solar wind during solar cycles 22–24. *Astrophys. J.* **751**, 128. DOI.

Manoharan, P.K.: 1993, Three-dimensional structure of the solar wind: variation of density with the solar cycle. *Solar Phys.* **148**, 153. DOI.

Manoharan, P.K., Ananthakrishnan, S.: 1990, Determination of solar-wind velocities using single-station measurements of interplanetary scintillation. *Mon. Not. Roy. Astron. Soc.* **244**, 691.

Manoharan, P.K., Kojima, M., Gopalswamy, N., Kondo, T., Smith, Z.: 2000, Radial evolution and turbulence characteristics of a coronal mass ejection. *Astrophys. J.* **530**, 1061. DOI.

Manoharan, P.K., Kojima, M., Misawa, H.: 1994, The spectrum of electron density fluctuations in the solar wind and its variations with solar wind speed. *J. Geophys. Res.* **99**, 23411. DOI.

Mejia-Ambriz, J.C., Jackson, B.V., Gonzalez-Esparza, J.A., Buffington, A., Tokumaru, M., Aguilar-Rodriguez, E.: 2015, Remote-sensing of solar wind speeds from IPS observations at 140 and 327 MHz using MEXART and STEL. *Solar Phys.* DOI.

Mejia-Ambriz, J.C., Villanueva-Hernandez, P., Gonzalez-Esparza, J.A., Aguilar-Rodriguez, E., Jeyakumar, S.: 2010, Observations of Interplanetary Scintillation (IPS) using the Mexican Array Radio Telescope (MEXART). *Solar Phys.* **265**, 209. DOI.

Moran, P.J., Ananthakrishnan, S., Balasubramanian, V., Breen, A.R., Canals, A., Fallows, R.A., Janhardan, P., Tokumaru, M., Williams, P.J.S.: 2000, Observations of interplanetary scintillation during the 1998 whole Sun month: a comparison between EISCAT, ORT and Nagoya data. *Ann. Geophys.* **18**, 1003. DOI.

Sajan, C., Mushini, P.T., Jayachandran, R.B., Langley, J.W., MacDougall, J.W., Pokhotelov, D.: 2012, Improved amplitude and phase-scintillation indices derived from wavelet detrended high latitude GPS data. *GPS Solut.* **16**, 363. DOI.

Scott, S.L., Coles, W.A., Bourgois, G.: 1983, Solar wind observations near the sun using interplanetary scintillation. *Astron. Astrophys.* **123**, 207.

Tokumaru, M., Kojima, M., Fujiki, K.: 2012, Long-term evolution in the global distribution of solar wind speed and density fluctuations during 1997–2009. *J. Geophys. Res.* **117**, A06108. DOI.

Tokumaru, M., Kojima, M., Fujiki, K., Maruyama, K., Maruyama, Y., Ito, H., Iju, T.: 2011, A newly developed UHF radiotelescope for interplanetary scintillation observations: solar wind imaging facility. *Radio Sci.* **46**, RS0F02. DOI.

Torrence, C., Compo, G.P.: 1998, A practical guide to wavelet analysis. *Bull. Am. Meteorol. Soc.* **79**, 61.

van Haarlem, M.P., Wise, M.W., Gunst, A.W., Heald, G., McKean, J.P., Hessels, J.W.T., de Bruyn, A.G., Nijboer, R., Swinbank, J., Fallows, R., *et al.*: 2013, LOFAR: the LOw-frequency ARray. *Astron. Astrophys.* **556**, 53. DOI.

Wannberg, G., Wolf, I., Vanhainen, L.G., Koskenniemi, K., Rottger, J., Postila, M., Markkanen, J., Jacobsen, R., Stenberg, A., Larsen, R., Eliassen, S., Heck, S., Huuskonen, A.: 1997, The EISCAT Svalbard radar: a case study in modern incoherent scatter radar system design. *Radio Sci.* **32**, 2283. DOI.